Study of Growth defects in Sapphire by Laser Rayleigh Scattering Imagining

Zewu Yan[1,2], Li Ju[1], Slawomir Gras[1], Chunnong Zhao[3], David G. Blair[1]

[1]School of Physics, The University of Western Australia, Nedlands, WA 6009, Australia
[2]Research Institute of Synthetic Crystals, Beijing 100018, P. R. China
[3]School of Computer and Information Science, The University of Edith Cowan

E-mail: yanzewu@hotmail.com

Abstract

We present the technique of laser Rayleigh scattering imaging (LRSI), which has been used for the mapping of inhomogeneities and point defects in sapphire test masses for laser interferometer gravitational wave detectors. We analyse errors associated with side wall mapping of cylindrical test masses, and present the comparison of two samples which show significant differences. The technique could be used to improve quality control in the manufacture of optical materials.

Keywords: Rayleigh scattering; sapphire test masses; gravitational waves; defect in crystals.

PACS number: 42.15. -i, 42.70.Km, 61.72.Dd, 78.30.Fs, 78.35. +i, 81.70.Fy

1 Introduction

Laser interferometric gravitational wave detectors require test mass materials with exceptional properties: very low acoustic loss, high Youngs' modulus, high thermal conductivity, high infrared transmittance and very high homogeneity. Sapphire is one of the most promising materials. However, it is difficult for manufacturers to grow large-size high-quality samples. Point defects and inhomogeneous structures in test masses can create sources of Rayleigh scattering and hence introduce noise and reduce the sensitivity[1,2,3,4]. It is an essential test to evaluated high-grade large sapphire test mass samples to ensure that an adequate low level of scattering is achieved.

We have previously[5] reported the investigation of inhomogeneous Rayleigh scattering in sapphire samples. Here we present a more detailed quantitative study of Rayleigh scattering using Laser Rayleigh Scattering Imaging (LRSI). This technique utilises a very sensitive cooled astronomical CCD camera to image the scattered light. This method allows an entire sample scattering map to be achieved. Images presented here show point defects and inhomogeneous structures in two cylindrical sapphire samples and emphasize the currently poor levels of quality control in sapphire growth.

2 Experimental Setup

In high quality optical materials the Rayleigh scattering signal is very low, typically a few ppm per cm. The scattered light has to compete with surface scattering and scatter from stray reflections. In addition scattering of a stray beam entering the camera optics can also overwhelm the Rayleigh scattering imaging. Various geometries for the mapping system have been investigated, but the best results have been from side scatter measurement, with a probe beam entering the end

face of a cylindrical sample. Even in this situation the scattered light from the face surfaces which are fine polished, but not anti-refection coated, prevents imaging within the first few millimetres of the cylinder ends.

Fig. 1 shows the experimental set up used for the measurements reported here. We studied two sapphire cylinders of 150mm diameter and 60mm thickness grown by the heat exchanger technique[6]. The incident beam of a He-Ne laser passes through the flat face of the sapphire sample along the y-axis. An objective lens focuses the scattering light onto a CCD camera (Meade Pictor 416 XTE CCD) at 90° (x-axis) to the laser beam. The distance between the laser beam and the camera is kept constant while the sample is moved on a computer controlled precision motion platform.

Due to the cylindrical shape of the sapphire samples, mapping the 90° Rayleigh scattering was done by moving the samples in cylindrical coordinates (R, θ). Imaging through the cylindrical surface leads to potential image distortions. This is discussed in section 3.

For the sample used here we tested a 60° imaging system in which the camera imaged through the front face of the sample at 60° relative to the laser beam. In this case the sample was moved through Cartesian coordinates. This avoids optical distortion. However we found that surface reflections from the flat surfaces overwhelmed the Rayleigh scattering information near the ends. This could be overcome by using anti-reflection coating on the samples. In this paper we will discuss only the case of 90° scattering as shown in Fig.1.

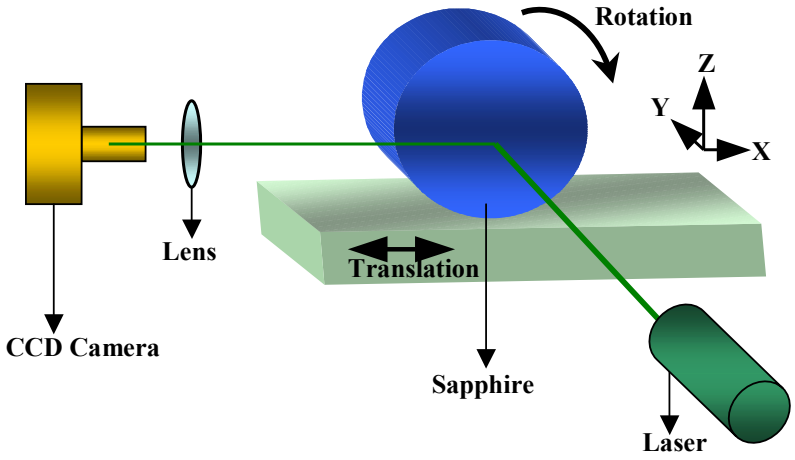

Figure 1 Schematic illustration of the experimental set-up

3 Image analyses

A typical CCD image of scattered laser beams through a sapphire sample is shown in Fig. 2. The images show the Gaussian laser beam profile modulated by the scattering level. The two bright spots S_1 and S_2 define the intersection of laser beam and the two surfaces of the sample. The bright areas nearby are the surface scattering peaks discussed above. The distance between S_1 and S_2 is the thickness of the sapphire. Determining this distance is important in calculating the Rayleigh scattering coefficient.

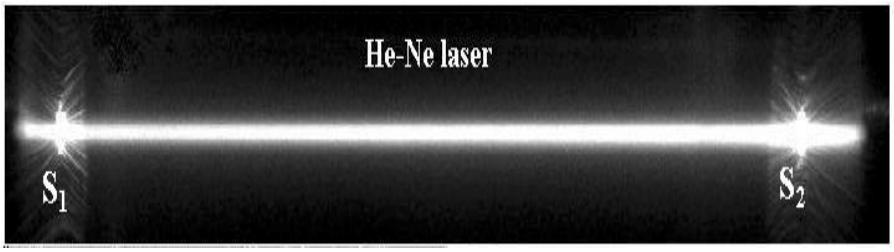

Figure 2 Image of the Rayleigh scattering light in the sapphire cylinder

Before discussing measurements we discuss the issue of imaging the laser beam through the cylindrical lens of the sapphire test mass wall.

Although the physical distance between the laser beam and the camera is fixed, the virtual position of the laser beam changes due to the cylindrical lens effect of the sample as the sample is moved, as shown in Fig.3a. Thus the image solid angle (and by extension the light intensity) seen by the CCD camera changes accordingly. From simple geometric optics, we can obtain equations for the distance s' of the virtual position of the laser beam from the cylinder surface, and Ω, the imaging solid angle defined in Fig. 3(a).

$$s' = \frac{n_2 R s}{R n_1 - s(n_1 - n_2)} \qquad (1)$$

and

$$\Omega = \frac{\pi \phi_{lens}^2}{4(L + s')^2} \qquad (2).$$

Here R is the radius of the sapphire sample, n_1 is the refractive index of sapphire, n_2 is the refractive index of air, s is the distance of the laser beam to the surface of the sapphire cylinder, and L is the distance between the sapphire cylinder surface and the lens.

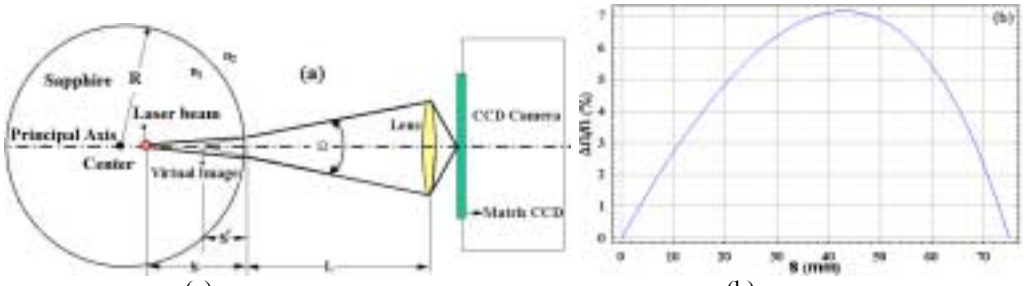

(a) (b)

Figure 3 (a) Schematic drawing of the imaging solid angle; (b) The fractional change of Ω with sapphire cylinder position

In the preceding equations, note that $L+s$ = constant. In our case, when the sapphire moves 75 mm, the relative change of the solid angle over this distance is shown in Fig.3b. It can be seen that, the maximum change is less than 8%. Correcting for the solid angle therefore only makes a small change in the results, so for the results presented below corrections have not been applied. Note however that the value Ω of diverges strongly when s exceeds more than half the sample diameter. For this reason the laser beam is never moved beyond the sample centre axis.

A second consideration is the focus of the camera. Although the distance between the CCD camera and the laser beam is a constant, the virtual image position of the laser beam will change with the sapphire's movement due to the lens effect of the sapphire cylinder. However measurements show that over the distance range used the images appear to be in sharp focus. This is expected as the depth of focus of the

camera is 60 mm. For this reason we have not corrected our measurements for changes in focus, which we believe to be negligible.

4 Results and discussions

4.1 Single beam scattering image

The experimental results are illustrated by the two characteristic single beam photographs in Fig.4. The left image from sample 1 has large point defects. The right image from sample 2 reveals a structure and a gradual change in beam width.

Images from the CCD are corrected by using dark frame and flat field correction. MATLAB software was used to process the CCD images. The corresponding 3D profiles of the images (shown in Fig.5) indicate fluctuations of the scattered light along the path or cross section. Point defects within the laser path can be easily detected.

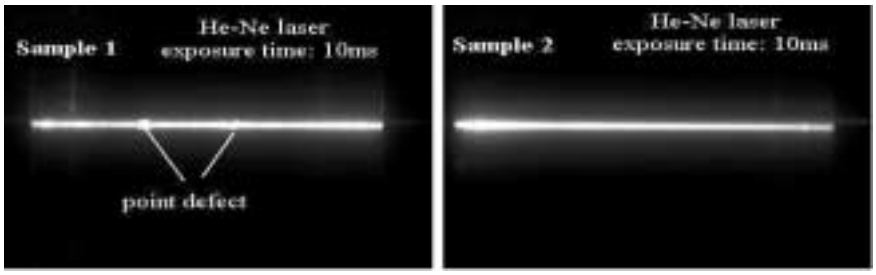

Figure 4 Characteristic images of Rayleigh scattering of a single laser beam in two samples

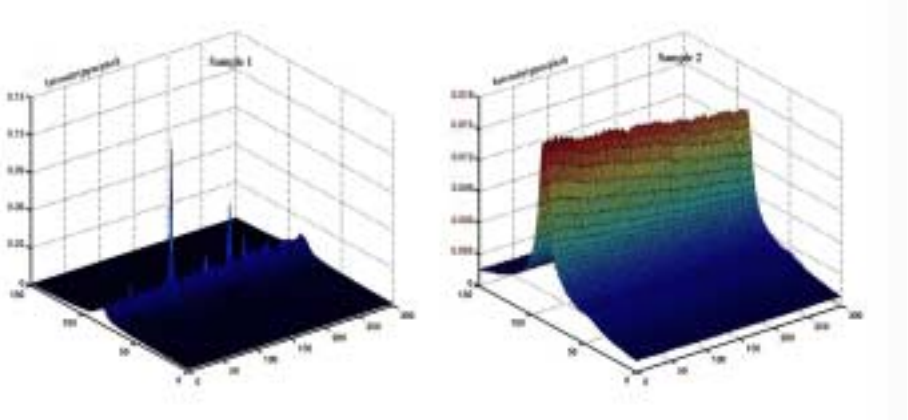

Figure 5 Comparison of intensities of Rayleigh scattering in two samples (note the difference in scales)

4.2 Rayleigh scattering coefficient

We used a previously calibrated sample to calculate the Rayleigh scattering coefficient[7] of these two sapphire samples. It can be seen from Fig.5 that the general maximum value of scattering intensity along the laser beam in sample 1 is less than 0.015 ppm/pixel except for the sharp peaks due to point defects with the scattering intensity up to 0.13 ppm/pixel. Sample 2 has a scattering intensity of 0.015-0.018 ppm/pixel. According to the wavelength dependence of Rayleigh scattering[7], it can be shown that the average Rayleigh scattering coefficient at 1064nm is about 4ppm/cm in sample 1 (not including point defects) and 7ppm/cm in sample 2, compared with 13ppm/cm previously reported in reference [8].

4.3 High resolution mapping of point defect

Fig.6 shows the detailed structure of one point defect in sample1. The scattering defects have dimensions larger than the 0.5mm laser beam. The defect shown here is about 1.5mm in diameter. This is significantly larger than the defect size when observed by a microscope. The scattering intensity is at least 20 times that of typical material.

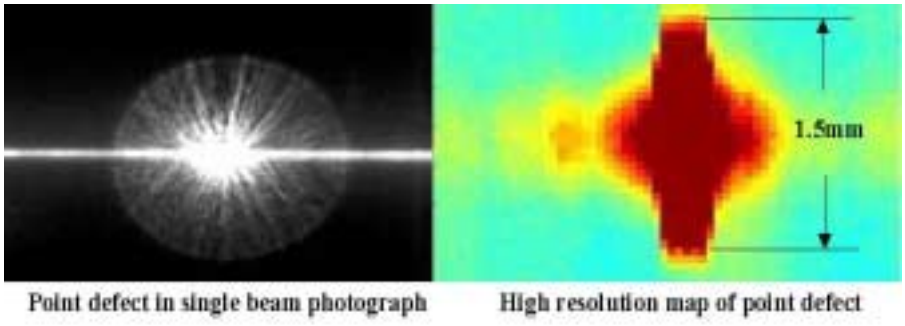

Figure 6 The detailed structure of one point defect in sample 1

4.4 Rayleigh scattering mapping of the samples

As mentioned above, the LRSI mapping of the cylindrical sample is realised by moving the sample in cylindrical coordinate (R, θ) relative to a fixed laser beam. The translation step within one layer is 0.5mm, about the size of the laser beam. The process of layer-by-layer mapping is shown schematically in Fig.7. Typically, mapping one section requires 100 scanning steps. Then the sample is rotated by successive θ degree interval around the centre axis of the sample to scan another section.

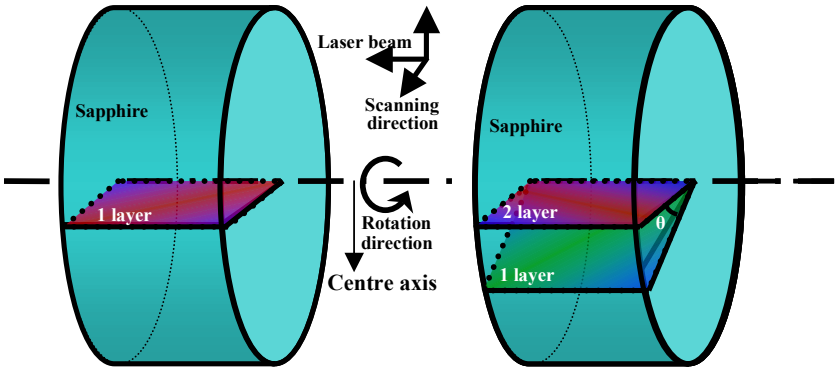

Figure 7 Illustration of mapping layer-by-layer Rayleigh scattering images within the test mass

The image of the Rayleigh scattering of a layer is created in two steps. First, a single beam image is converted into a one-dimensional array defined by the peak intensity values. Second, the set of arrays for multiple beam images is combined to give a 2D or 3D image array. Fig. 8 shows six scanned layer maps from sample1 with large point defects in each layer. Fig. 9 (a) shows the six scanned layer maps from sample 2 which shows a large scale inhomogeneous structure. The horizontal lines are artefacts. Reconstructing two layers of the scanned images into the cylinder sample (Fig. 9), it can be seen clearly that sample 2 has a roughly cone shaped structure. This is not surprising as it is likely to be due to non-uniform crystal growth or impurities in a heat exchange crystal growth crucible.

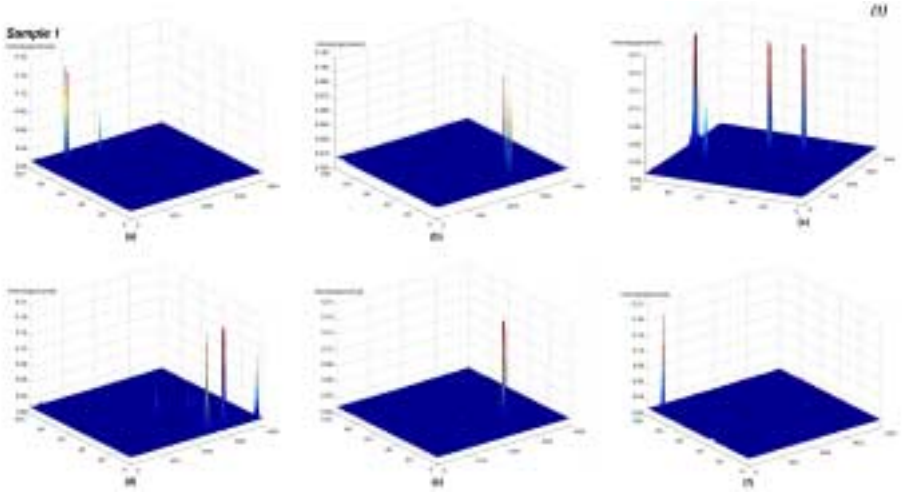

Figure 8 Six layers (18 °) apart of Rayleigh scattering images of sample 1 with point defects best shown as 3D plot.

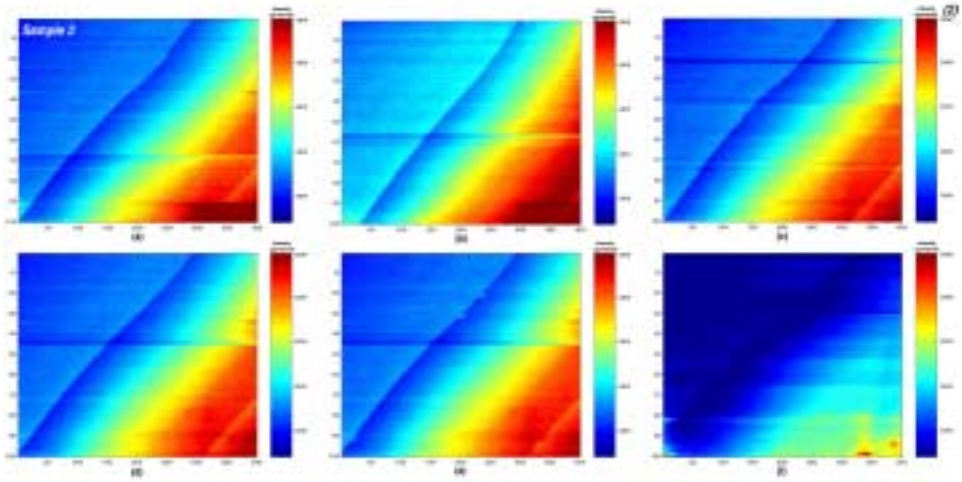

(a)

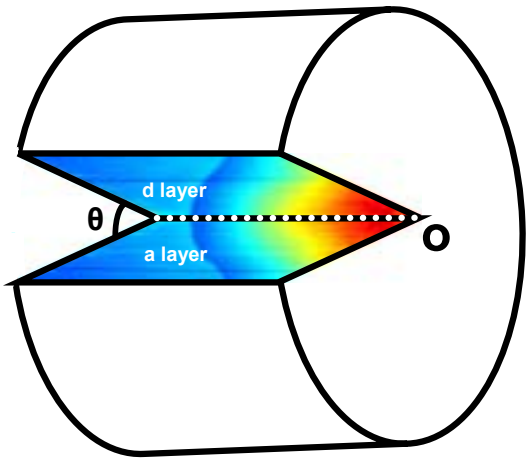

(b)

Figure 9 (a) Six layers (18° apart) of Rayleigh scattering images of sample 2 best presented as 2D plot, showing inhomogeneous structures. (b) The cone inhomogeneous structure in sample 2.

5 Conclusions

Laser Rayleigh Scattering Imaging provides a method for quantitative high resolution mapping of inhomogeneities in optical materials. The process of mapping entire cylindrical test masses is amenable to automation.

Point defects and inhomogeneous structures in the single sapphire crystals were clearly revealed by Laser Rayleigh Scattering Imaging. The average Rayleigh scattering coefficient at 632.8nm is about 4ppm/cm in sample 1 and 7ppm/cm in sample 2.

The LRSI technique may provide data that can be utilized to improve the quality control of both single crystal and glass optical materials. The resolution of the current setup is limited by the laser beam size. Further work will improve the resolution of the technique so that it can be used to detect dislocation lines or loops in crystals.

6 Acknowledgments

The authors would like to thank Pablo Barriga in assisting on the automation of precision motion platform. We would like also to thank the LIGO Science Collaboration core optics group, especially GariLynn Billingsley and David Reitze for support and useful discussions through regular teleconferences. This work is supported by the Australian Research Council, and is part of the Australian Consortium for Interferometric Gravitational Astronomy.

References

[1]. W. Winkler, K. Danzmann, A. Rudiger et al 1991, *Phys. Rev.* A 44, 7022-36
[2]. J. Gamp 1997, *LIGO Rep.* LIGO-T970074-00-D
[3]. Y. Vinet, B. Meers, C. N. Man et al 1988, *Phys. Rev. D* **38**, 433-47
[4]. Y. Vinet, V. Brisson, and S. Braccini 1996, *Phys. Rev. D* **54**, 1276-86
[5]. Z. Yan, L. Ju, F. Eon et al 2003, *Class. Quantum Grav.* **21**, S1139 - S1144
[6]. Crystal Systems, http://www.crysys.com/hem.html
[7]. B.Chu, Laser Light Scattering (Academic Press, New York, 1974)
[8]. F.Benabid, M.Notcutt, L. Ju et al 1999, *Opt. Commun.* **167**, 7-13